



SPE 90336

## Multiscale Flow and Transport in Highly Heterogeneous Carbonates

Liyang Zhang, SPE, Steven L. Bryant, SPE, James W. Jennings, Jr., SPE, Todd J. Arbogast, SPE, The University of Texas at Austin, Ramoj Paruchuri, SPE, Landmark Graphics Corporation

Copyright 2004, Society of Petroleum Engineers Inc.

This paper was prepared for presentation at the SPE Annual Technical Conference and Exhibition held in Houston, Texas, U.S.A., 26–29 September 2004.

This paper was selected for presentation by an SPE Program Committee following review of information contained in a proposal submitted by the author(s). Contents of the paper, as presented, have not been reviewed by the Society of Petroleum Engineers and are subject to correction by the author(s). The material, as presented, does not necessarily reflect any position of the Society of Petroleum Engineers, its officers, or members. Papers presented at SPE meetings are subject to publication review by Editorial Committees of the Society of Petroleum Engineers. Electronic reproduction, distribution, or storage of any part of this paper for commercial purposes without the written consent of the Society of Petroleum Engineers is prohibited. Permission to reproduce in print is restricted to a proposal of not more than 300 words; illustrations may not be copied. The proposal must contain conspicuous acknowledgment of where and by whom the paper was presented. Write Librarian, SPE, P.O. Box 833836, Richardson, TX 75083-3836, U.S.A., fax 01-972-952-9435.

### Abstract

Large-scale (cm and greater) heterogeneities raise both practical and theoretical problems for understanding fluid flow through rocks that contain them. Standard sampling methods such as thin sections, core plugs, and even whole core are at a scale too small to resolve these heterogeneities, and direct measurement of flow properties is not straightforward. Moreover it is not obvious what physical formulation (e.g., Darcy's law, Forchheimer's Law, Stokes flow) is appropriate for modeling flow or interpreting flow measurements, nor is it clear that traditional homogenization approaches (e.g., effective medium theory, renormalization, dual-porosity) are applicable in such systems. We report simple measurements on a large 25 cm diameter by 36 cm high sample of Cretaceous carbonate containing centimeter-scale vugs, and compare them to flow fields computed from high-resolution CT images of the same sample. These computations use a single-physics Darcy-flow model. We also compute passive tracer transport in the same model to evaluate preferential flow paths within the rock. The direct computations are based on a porosity grid extracted from a set of CT images ( $512 \times 512 \times 240$  pixels, 0.5 mm resolution) of the large sample. We also use the single-physics model to estimate the length scale of connections between vugs in this sample. The results demonstrate the need for upscaling methods that preserve connectivity of features in highly heterogeneous rocks.

### Introduction

Fluid flow in carbonates is important geologically, as it controls the circulation of diagenetic fluids, and economically in the movement of groundwater and recovery of hydrocarbons. Carbonate rocks contain more than 50% of the world's hydrocarbon reserves, and although not all of these reservoirs contain vuggy pore systems, understanding the

physics of flow in such systems is an important problem. It is however a challenging problem because the pore space of carbonates evolves in a complex manner over time through the occlusion of primary porosity by cementation, and the development of secondary porosity by dissolution. The diagenesis of carbonates combined with other geological effects can result in extremely heterogeneous rocks.

Vugs are particularly challenging to deal with as the relative heterogeneity they introduce can vary widely. A vug is a cavity, void or large pore in a rock. Lucia presents a classification of vuggy pore space based on vug interconnections. He considers two types of vugs: separate-vug pores and touching-vug pores [1]. The vugular fabrics include a variety of pore types that generally fall into two groups. The first group is composed of non-tectonic fractures, karst conduits, caverns and collapse breccias, and it is normally associated with karsting and massive dissolution. The second group is composed of interconnected molds that are associated with selective dissolution of fossil fragments or voids within or between fossils that were never filled in by sediment [1]. The rock fabric of interest in this research is the second group, a multiscale structure system. These types of multiscale heterogeneous systems are difficult to study mostly because the heterogeneity is on a scale that is too large to be captured by standard core samples. In this research, we are most interested in the connectivity characteristics of the vugs. The focus of this study is to understand how cm-scale vugs influence flow and transport behavior at the 10 cm to 1 m scale. To do so we combined numerical calculation on a high-resolution (mm scale) X-ray Computed Tomography image of a large sample with physical experiments on the same sample.

Results from the physical experiments will improve the confidence in physical model(s) used for the numerical simulation. The complex geological features of the target sample indicate that simulating samples with different degrees of connectivity between the vugs would be instructive. The ultimate goal of this research is to develop models that predict the effective flow properties of highly heterogeneous carbonates.

### Rock Sample

**General introduction.** The rock sample used for the test was collected from the Pipe Creek Reef, a caprinid buildup in the Glenn Rose Formation near the town of Pipe Creek, Texas [2]. The sample is a Cretaceous limestone with large fossil fragments, inter-fossil voids and intra-fossil moldic pores. The

sample was broken from the outcrop and trimmed to fit within the CT scanner. It is irregular in shape, but roughly a cylinder of 25cm in diameter and 36cm in height. The sample was scanned with an industrial high-resolution X-ray computed tomography (CT) scanner at The University of Texas, Department of Geological Sciences. Compared with medical scanners, this instrument operates at higher energies with configurable source and detector geometries, making it capable of scanning high-density objects with higher resolution [3]. The Pipe Creek sample was scanned with 240 slices, with thickness 1.5mm. Each slice was reconstructed with  $512 \times 512$  pixels, each of which is a square with sides 0.543 mm by 0.543 mm.

Images of two selected slices from the sample are shown in Figure 1. Lighter shades in the images indicate denser materials. In this case, this part is the rock matrix. The darkest shades indicate lightest materials, which correspond to vugs. The intermediate density shades show the vugs are partially filled by recent sediment, when the rock was exposed in the creek bed.

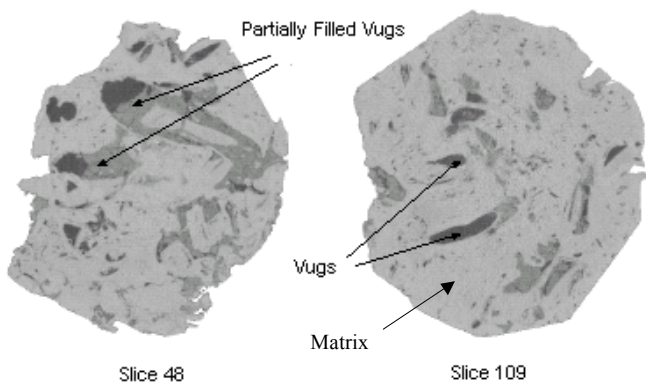


Fig. 1. CT scans of the carbonate rock sample

**Sub-samples.** After the CT scan, the rock was cut into two sub-samples (Fig 2). The smaller sub-sample is approximately 11 cm in length. The larger sub-sample is the remaining part of the entire sample and is about 25 cm in length. Henceforth, these sub-samples are referred as the *small sample* and the *big sample* for convenience.



Small Sample

Big Sample

Fig. 2. Two rock sub samples

## Experimental Methods

The following two sections explain the laboratory experiments that were conducted on the *small* and *big* samples. The main objective of these experiments is to find the effective permeability of the rock.

### 1. Small sample

**Experimental method.** As shown in Fig. 2, the *small sample* has very irregular shape and has many large vugs on the surface. Flow experiments on this sample were conducted by placing the sample onto a bed of sand within a large (five gallon) bucket. Screens were wrapped around the sample, and sand was placed in the annular space. The flow experiment was conducted by supplying water at a constant head. Fig. 3 shows the experiment apparatus.

**Experiment apparatus.** As shown in Fig.3, a bucket was prepared by drilling some evenly distributed small holes in the bottom, which allowed the water to flow out with negligible

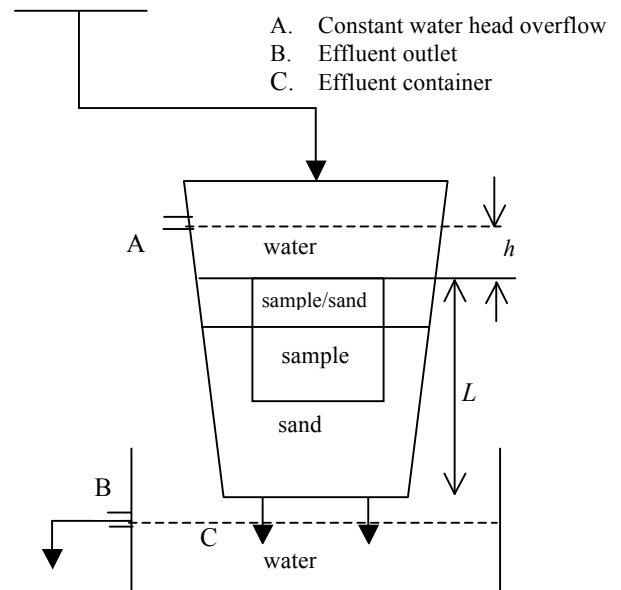


Fig. 3. Small sample experiment apparatus

resistance. Six layers of small mesh screens were placed onto the bottom of the bucket to prevent sand from falling through the bucket holes. Measurements showed that the screens also provided negligible resistance to flow. The bucket was then filled about half-full with coarse sand. Water was flowed through the sand to ensure that it was well packed. The *small sample* was first wrapped with two layers of the screen materials to prevent sand entering into the vugs, before placing it onto the sand pack in the bucket. A rubber ring with about 24cm size opening in the center was placed between the sand pack and the sample to prevent preferential flow through the annulus between the sample and the bucket. This annulus was then carefully filled in by sand and was packed in the same way as before. The bucket and approximate sample dimensions are listed in Table 1, which is shown in Appendix I. Table 2 shows the grain size distribution for the sand.

**Experiment principle.** Constant water head at the inlet was established by means of an overflow port *A* located a few cm above the top of the sample. Effluent water was collected from overflow port *B* through a large container, in which the bucket was placed. The flow measurements were conducted on the combined sand and *small sample* system with length *L* as shown in Fig. 4. This system is referred as *combined system* for the small sample in the following of this paper. Steady state flow rates for different water heads were calculated by collecting the effluent for certain periods of time. The effective permeability for the *combined system* was calculated using Darcy's Law. Formula (1) gives the effective permeability of the *combined system* with bucket geometry, from which the sample permeability was estimated as shown in Appendix II.

$$k_{avg} = \frac{quL}{\pi R_1 R_{out} \rho g (h + L)} \quad (1)$$

where

$R_1$  bucket inner radius right on top of the tested system

$R_{out}$  outlet tested system radius (rubber ring radius)

$L$  length of the tested system

$h$  water head above top of sample

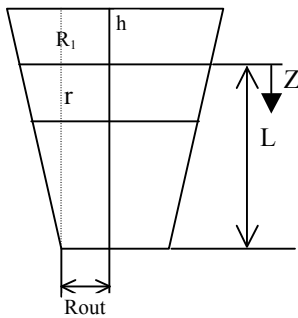


Fig. 4 Geometry sketch of the flow system

**Experiment results and analysis.** Table 3 in Appendix I shows the experimental results for the *small sample*. Setup 2 and 3 in the table were the two special sets of measurements, in which a section of sand was put on top of sample for setup 2 and impermeable wax was filled around the annulus for setup 3. The sample permeability in the table is calculated as shown in Appendix II. The effective permeability ranged from 95 darcy to 151 darcy for these different experimental conditions.

The most important observation from these experiments is that the effective permeability is very large, on the order of 100 darcy. The large permeability result suggests that the vugs in this *small sample* are connected. The large size vugs, as shown in the picture (Fig. 2) may also cause large permeability. Both good vugs connections and their large size can contribute to large conductivity of the sample.

## 2. Big sample

**Experimental method.** The *big sample* has smaller vugs seen on the surface than on the *small sample* and the shape of the sample is closer to cylindrical though it is still irregular. A

preliminary experiment was conducted on this sample using the same setup described above for the *small sample*, with sand filling in the annulus between the sample and the bucket. In this preliminary experiment, meaningful values of permeability could not be obtained. It was concluded that the flow was mainly going through the sand in the annulus space, rather than through the sample. Unlike the *small sample*, sealing the outer surface of the *big sample* was feasible, and indeed it was the only way to force flow through the rock. Although the roughly cylindrical geometry makes it possible to seal the rock, the irregular shape, the rough surface and the intersection of large vugs with the surface made it difficult to achieve a strong seal. Materials such as shrink tube, silicon caulk, plasti-dip, wax etc. were tested on the *big sample*. Air lock, a material used on air conditioning ductwork, was the best seal found for the *big sample* so far. The seal was thick and strong enough to stick on the rock surface without entering the vugs.

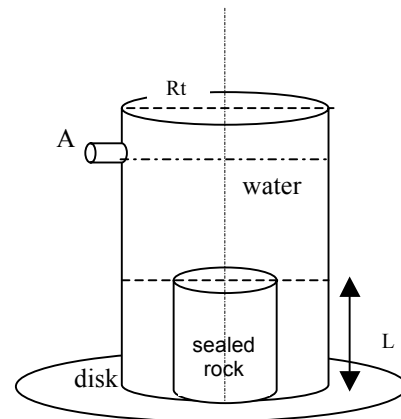


Fig. 5 Big rock experiment apparatus

**Experiment apparatus.** The *big sample* with air lock seal was put into a large-diameter PVC pipe as shown in Fig. 5. The flat bottom face of the sample was sealed to a Lucite disk with a hole in the center slightly smaller than the diameter of the rock. The pipe was placed and sealed onto the larger diameter disk, on which the rock sample was sealed. Thus the annulus between the *big sample* and the pipe was sealed at the bottom of the pipe. The bottom of the rock was open to an effluent container as for the *small sample*. Steady state experiments were conducted by supplying inlet water at a rate sufficient to cause overflow through outlet *A*.

**Experiment principle.** The effective permeability of the *big sample* is directly calculated from Darcy's law for this setup.

**Experiment results and analysis.** The permeability measured for the *big sample* was approximately 35 mD, which is about 3000 times smaller than 100 darcy measured for the *small sample*. The small permeability may be caused by smaller vug sizes or narrower connections through the *big sample* compared to the *small sample*. Although we attempted to remove the modern river sediment from the sample by high-pressure washing, flow through the vugs and their connections may have been restricted by small amounts of remaining mud. Sediment was observed to settle on the bottom of the effluent container during the experiments both for the *small* and the

*big sample*, indicating that at least small amounts remain in the samples. This is consistent with the partially mud-filled vugs detected from CT scan. It is also possible that the vugs in the *big sample* had no inter-connections. The measured effective permeability would thus be dominated by the matrix permeability.

We further investigate the observations made in the laboratory experimentation by modeling the *small sample* with the bundle of capillary tubes technique and by numerically simulating the *big sample*.

## Mathematical and Computational Modeling

### 1. Small sample

**Capillary model.** The connectivity of the vugs in the *small sample* was tested using a simple bundle-of-capillaries model to represent vugs or a series of connected vugs.

The *small sample* was considered as bundle of capillary tubes with impermeable matrix. The capillary tubes in this model are imagined as the connected vugs.

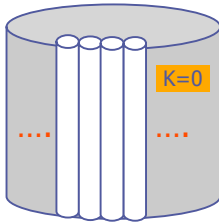


Fig. 6 Capillary tube model

The effective permeability of the sample is calculated based on steady state assumption using Hagen-Poiseuille's Law and Darcy's Law. For straight tubes with the same size of radius  $r$ , the rock permeability is calculated using Formula (2).

$$k = \frac{\phi r^2}{8} \quad (2)$$

**Calculation and analysis.** The model calculations were based on the system dimensions of experiment 3 (Table 3) with cylinder geometry approximation for the *combined system*. The average permeability of this experiment (124 darcy) was used as the reference permeability. The permeability of the rock sample was first determined from the capillary model. The average permeability of the *combined system* was then calculated, which is called model average permeability in this section. The results are shown in Fig.7 attached in Appendix I.

The plots in Fig.7 show the *combined system* permeability versus the capillary tube radius for different numbers of capillary tubes. The experiment reference permeability (124 darcy) and the sand permeability (135 darcy) are also plotted. As can be seen, the *combined system* permeability with no tubes is a about 70 darcy, the permeability of the system with an assumed impermeable rock surrounded by 135 darcy sand. All the other lines become constant at a permeability of about 200 darcy when the capillary tube radius is large enough. Thus, when the effective permeability obtained from capillary model is large, the apparent permeability of the *combined system* is dominated by the permeability of the sand.

The key feature of this plot is the intersections of the reference permeability line with the model average permeability lines. For example, the meeting point of the reference permeability line with the 10,000 tube model average permeability line corresponds to a capillary tube radius of about 200 microns. It means that the average permeability of 124 darcy for the *combined system* would be measured if the rock was equivalent to a bundle of 10,000 capillary tubes of radius 200 microns. Similarly, 2000 microns tube radius can be obtained for the case of a single capillary tube. However, the largest vug size seen on the top of the *small sample* is in the order of 1 cm in radius. A capillary tube model of this size would give a much larger average permeability than 124 darcy. This suggests that the large channel apparent at the surface must become narrow inside the rock. Another way to view this result is that the vugs in the *small sample* must be connected by relatively narrow channels.

This conclusion also holds if we allow for the possibility of turbulent flow within the tubes. The plots are shown in Fig. 8 in Appendix I. Comparisons of calculation results of turbulent flow with laminar flow in Fig. 8 show that the average permeability for the *combined system* remains the same.

### 2. Big sample

**Numerical simulation.** The computation grid for flow simulation is available from the interpretation of the 3D computer CT scanned images. Single-phase flow and transport simulations were performed using ParSSim on the *big sample*, which are explained below.

**Simulator.** Parallel Subsurface Simulator (ParSSim) was used in this simulation. The Passim code was developed by the Center for Subsurface Modeling (CSM) of the Institute for Computational and Engineering Sciences (ICES) at the University of Texas at Austin. It is an aquifer or reservoir simulator for the incompressible, single-phase flow and reactive transport of subsurface fluids through heterogeneous porous media. Simulations in this research project use the flow and transport functions of ParSSim [4]. Darcy flow is used initially in the simulator. Using Stokes flow in vugs and Darcy flow in matrix in computation might give more accurate results for flow through this vugular system, which is also the research of interest in the future, but Darcy flow simulation will give invaluable information at the first step.

**Single phase flow calculation.** For convenience in applying boundary conditions within the simulator, a 3D rectangular box sub-sample was extracted from the center of the whole CT scan. The sub-sample is about 1/3 of the entire rock volume. The 0.5 mm × 0.5 mm × 1.5 mm pixels in the scan were mapped to cells in the computational grid. Each cell was categorized as rock matrix, vug, or vug containing recent sediment. Porosity values were assigned to individual cells according to the CT density in the matrix cells. Vugs and vugs with mud were assigned 100% porosity. Permeability of the cells in vugs was assigned a large arbitrary value (in orders of darcy). The objective in these calculations was to determine whether the vugs were connected and how the overall permeability depended on vug permeability and vug inter-

connectivity. For this purpose, assigning a constant small value (1 mD) to the matrix cells was sufficient.

The computational grid for the sub-sample directly mapped from CT scan is called 0 level, which has  $240 \times 240 \times 144$  cells. Upscaling from fine scale to coarse grid was useful for reducing the computation time. The 0 level is upscaled to level 1 by a factor of  $3 \times 3 \times 1$  into  $80 \times 80 \times 144$  cells. That means each cell in level one includes  $3 \times 3 \times 1$  neighbor fine grids from 0 level. By performing  $3 \times 3 \times 1$  up-scaling, the grid cells in the first level become cubes 1.5 mm on a side. After the first level, each higher level (from 2 to 16) was upscaled by  $2 \times 2 \times 2$  from the previous level. In this way the cells remain as cubic for all the upscaled levels. The different scale up levels and corresponding grid cells are shown in Table 4 in Appendix I. Studies were conducted on different levels to illustrate the importance of proper upscaling and using coarse grids. The proper upscaling will provide the appropriate effective permeability without losing key features of the micro-media, mainly the connections of the vugs [5]. The properties (porosity and permeability) for upscale levels are calculated from 0 level using arithmetic and 1/3 power averages, respectively.

Constant potential boundary conditions are set up for one pair of faces (inlet and outlet) of the rectangular sub-sample and a no flow condition is specified to the other faces. For transport calculations, the tracer concentration is fixed at unity at the inlet face. The flow computation results are shown in Fig. 9 & Fig.10 in Appendix I. Both of them are obtained with assigned matrix permeability 1mD. In these calculations, we assigned permeability of vugs containing mud as if no mud were present. The objective was to simulate the physical sample condition under (deep) subsurface conditions, where no mud is present. Hence only two categories of permeability are assigned on 0 level CT scan grid cells – vugs and matrix.

Fig. 9 shows the effective permeability in x, y and z directions with assigned vug permeability 10 darcy for four upscale levels. It is easy to see from the graphs that the permeability is anisotropic for this sample because the permeabilities in x, y and z directions are different. The graphs also show that the permeabilities are different for different scale up levels. These calculations show that local power averaging does not preserve fine scale vug connectivity. Topology, the connections between features, must be accounted for to obtain a good estimate of effective permeability.

Fig. 10 plots x direction effective permeability ( $k_{eff\_x}$ ). Since the plots of y and z direction permeability ( $k_{eff\_y}$  and  $k_{eff\_z}$ ) are similar to that of  $k_{eff\_x}$ , only the latter one was attached in this paper. The dimensionless effective permeability to matrix in this plot has a very clear increasing tendency with dimensionless vug permeability for all scale up levels. This means the larger the assigned vug permeability, the larger the calculated effective permeability. This indicates that vugs must be connected in this sample. If there were no connections between vugs, the permeability increase in the isolated voids would have little effect on the effective permeability of the sample. This was a useful finding, because the complexity of the CT image made it impossible to determine by inspection whether the vugs were connected.

Fig. 10 also shows that the effective permeability is about 2 orders of magnitude smaller than the permeability value assigned to the vugs. This suggests that the effective permeability of the sample is dominated by some small conductivity regions. A simple calculation was made on this sample by assuming there was one vug (tube) with radius 0.2 mm going through the impermeable matrix. The effective permeability of this system was obtained as about 40 md, which is in a similar magnitude of measured effective permeability 35 md. Apparently there is far more than one vug of 0.4 mm diameter in this sample (Fig. 2). The impermeable matrix assumption is also not realistic. The effective permeability of the *big sample* must be much larger than 35 md if all the vugs were well connected. Therefore, the channels between the vugs in the *big sample* must also be constricted as those in the *small sample*. But the constrictions in the *big sample* must be much narrower than those in the *small one* due to smaller permeability measurement (35 md).

These findings show that the connectivity of vugs in this sample is scale dependent. The vugs in the *small sample* have better connections, which give larger vug conductivity and thus larger sample effective permeability. Compared to the *small sample*, the vugs within the *big sample* have poorer connections, which give smaller vug conductivity and thus smaller sample effective permeability. Therefore the conclusion can be made based on these two sub-samples that the larger the sample, the poorer the connection is.

**Topologically-consistent permeability averaging.** An up-scaling technique when applied to permeability data is appropriate when it preserves the flow effects of the fine-scale features. In Fig. 9, it is clear that  $k_{eff\_z}$  is consistent with the scaleup. This topologically consistent effective permeability obtained by the 1/3 power averaging can be attributed to the normal distribution of the vugs and well defined inter-connections between the vugs along the z direction. Also, we can observe up to a 20% variation in the effective permeability after the scale-up along the other directions in the same figure, but in Fig. 10 we can see this scaleup method preserves the vug size effect on the  $k_{eff\_x}$  and not the topologically dependent features. Efforts to develop simple, topologically-aware local averages have yielded some success on model systems based on the Pipe Creek sample [6].

**Transport calculation.** As mentioned earlier, the concentration boundary conditions are set up for one pair of flow direction faces on the 3D sub-sample. A tracer transport simulations were performed to understand the preferential flow path through the rock. The computation conditions are consistent with those for flow, that is assigning vug permeability as 10 darcy and matrix permeability as 1mD. The numerical result of transport in z direction on 8<sup>th</sup> upscale level is attached as in Fig. 11 as well as the analytical solution of the classical 1-D advection/dispersion equation.

Fig. 11 shows the computed effluent tracer concentration as a function of pore volumes injected and the analytical solution for a homogeneous medium with Peclet number 5. The numerical solution shows tracer breakthrough much earlier than 1 PV. This is consistent with rapid tracer transport through some preferential flow paths (series of vugs). As shown in Fig.11, the analytical solution with Peclet number 5

is close to the computed effluent history for later times, but does not predict the early breakthrough.

An exact match of the analytical solution with the numerical solution could not be obtained for this sample. Smaller Peclet numbers yield earlier breakthrough times but underpredict the tail at later times. Evidently the range of travel times along the flow paths in the upscaled sample is so broad that an effective dispersion coefficient cannot be defined. It is impossible to model the solute transport in the heterogeneous sample by an equivalent homogeneous system with a single value of dispersivity.

## Conclusions

The vugs in this sample appear to be connected by narrow channels. Measurements of steady state single-phase flow indicate that the flow paths pass through constrictions much narrower than the vugs themselves. Both the *small* and the *big* sample studies show the vugs have narrow connections, though the connections in *small sample* might be larger than those in the *big sample*.

The connections are scale dependent. Better connections appeared in small-scale sample and poorer connections appeared in large-scale sample.

Because vug connectivity is scale dependent, the effective permeability is likewise scale dependent. The studies on this sample show that the larger the sample, the smaller the permeability.

Tracer transport simulations show that the degree of heterogeneity of the rock sample is too large to be modeled by a single value of overall dispersivity.

## Acknowledgements

This research was supported by the NSF (DMS0074310) and by the Industrial Associates of the Reservoir Characterization Research Laboratory, Bureau of Economic Geology, The University of Texas at Austin. We are also grateful to Mark Anderson for allowing us access to his property and to Charlie Kerans and Tom Fett for assistance with field work at the Pipe Creek outcrop.

## References

1. Lucia, F. J., 1999, *Carbonate Reservoir Characterization*, Springer-Verlag, New York.
2. Perkins, Bob F., 1974, Paleocology of a rudist reef complex in the Comanche Cretaceous Glen Rose Limestone of Central Texas; in Perkins, Bob F., ed., *Aspects of Trinity Division Geology, Geosciences and Man*, LSU, v.8, pp.131-174.
3. Ketcham, R.A. and Carlson, W.D., Acquisition, optimization and interpretation of X-ray computed tomographic imagery: Applications to the geosciences. *Computers and Geo-sciences*, 27(2001) pp. 381-400.
4. T. Arbogast, User's guide to Parssim1: The parallel subsurface simulator, single phase, in multiphase flows and transport in porous media: State of the art, Z. Chen, R.E. Ewing, and Z.-C. Shi, eds., *Lecture Notes in Physics*, Springer, Berlin, 2000.  
<http://www.ices.utexas.edu/~arbogast/parssim/>
5. T. Arbogast, D. S. Brunson, S. L. Bryant, and J. W. Jennings, Jr., A preliminary computational investigation of a macro-model for vuggy porous media, in *Proceedings of the conference Computational Methods in Water Resources XV*, C. T. Miller, et al., eds., Elsevier, 2004.
6. Ramoj K. Paruchuri, *Modeling Flow and Transport in Heterogeneous Media*, Master's Thesis, The University of Texas at Austin, 2003.

**Appendix I: Tables and plots**

Table 1 Dimensions for Bucket and Rock

ID bucket at Top (cm)	29.3
ID bucket at Bottom (cm)	26.1
OD bucket at Top (cm)	29.6
OD bucket at Bottom (cm)	26.4
Bucket Thickness (cm)	0.3
Approximate Dimnesions for Rock Sample	
Height (cm)	10.5
Diameter at Bottom (cm)	24

Table 2 Grain Size for Sand F35

d (um)	weight (g)	percentage(%)
425	85	46.3
297	87.3	47.6
250	7.7	4.2
210	1.2	0.7
180	1.2	0.7
150	0.4	0.2
<150	0.6	0.3
<b>Total</b>	<b>183.4</b>	

Table 4 Upscaling table

Scale-up Level	NxXNyXNz	Total Cells
0	240 X 240 X 144	8294400
1	80 X 80 X 144	921600
2	40 X 40 X 72	115200
4	20 X 20 X 36	14400
8	10 X 10 X 18	1800

Table 3 Experimental Results

Run	Rock and Sand							
	Sand Only		Setup 1				Setup 2	Setup 3
	1	2	3	4	5	6	7	8
Water head h (cm)	11	2	4.5	9	15.5	18	3.5	8
Sandpack length L1 (cm)	23	32	19	14.5	8	5.5	20	15.5
Rock height L2 (cm)	-	-	10.5	10.5	10.5	10.5	7	5
Sandpack/air and rock length L3 (cm)	-	-	-	-	-	-	3.5	5.5
Apparent permeability of the entire system(d)	135	135	124	124	141	134	146	132
Average permeability of the section contains the rock(d)	-	-	106	110	147	134	121	68
Effective permeability of the rock(d)	-	-	95	102	151	134	113	109

Fig.7 Average permeability of the entire system vs. tube radius for laminar flow

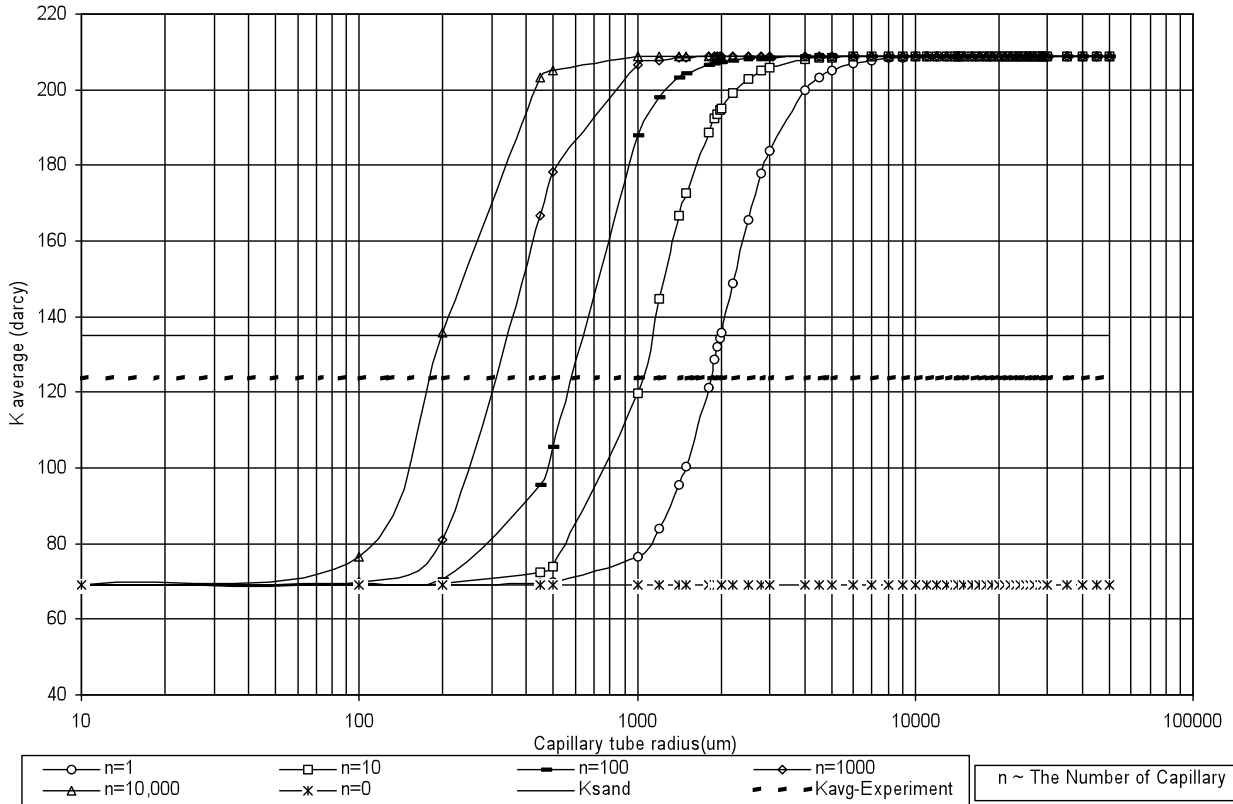


Fig.8 Average permeability of the entire system vs. tube radius for turbulent flow

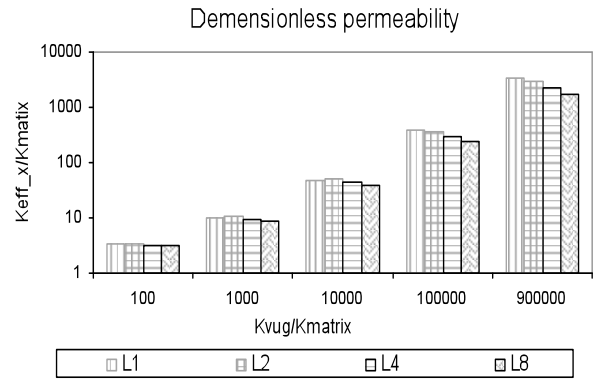
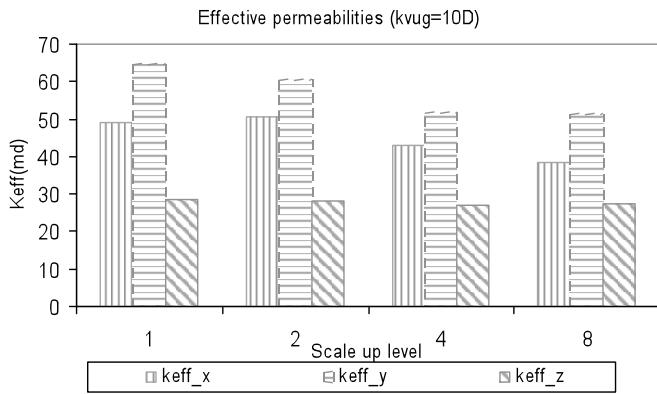
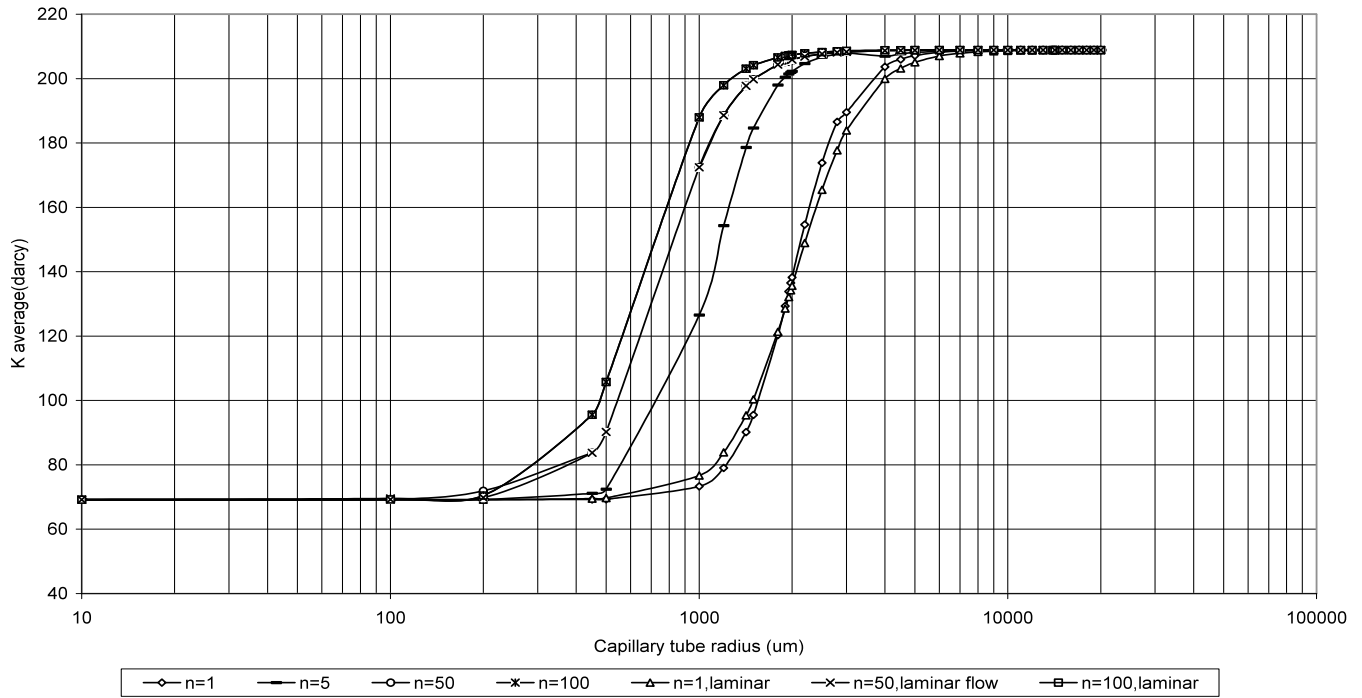


Fig.9 Effective permeability for different scale up levels

Fig. 10 Dimensionless permeability

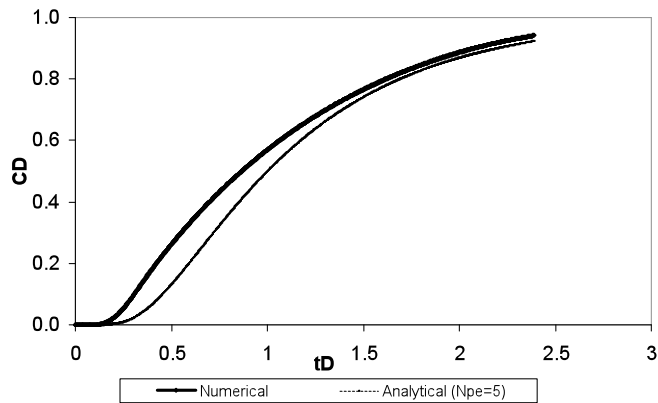


Fig. 11 Effluent tracer concentration vs. pore volume injected

## Appendix II. Rock Permeability derivation on small sample.

In order to get rock permeability, the test system was considered as three sections as shown in Fig.A1. The average permeability of section 2 was calculated from the Harmonic average as shown in formula A1. The bucket geometry was also included in this calculation.

$$k_2 = \frac{L_2}{R_2 R_3 \left( \frac{L}{k_{avg} R_1 R_{out}} - \frac{L_1}{k_1 R_3 R_{out}} - \frac{L_3}{k_3 R_1 R_2} \right)} \quad (A1)$$

where  $R_1$ ,  $R_2$  and  $R_3$  are top radius for sections 3, 2 and 1 respectively.  $R_{out}$  is the outlet system radius. The length and permeability of each section are denoted accordingly as shown in Fig. A1. The total *combined system* length is  $L = L_1 + L_2 + L_3$ .

The rock permeability was then calculated from formula A2 by systems in parallel in section 2.

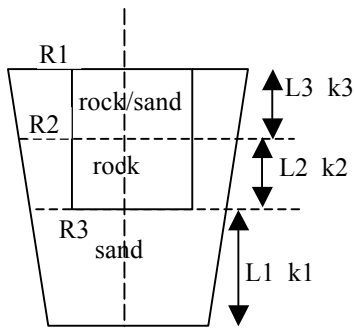


Fig. A1 Cross section sketch for rock permeability calculation

$$k_r = \frac{k_2 A_{2avg} - k_{annulus} A_{annulus}}{A_r} \quad (A2)$$

where  $A_{annulus}$  is the annulus area between rock and bucket;  $k_{annulus}$  is the permeability of the annulus, which is sand permeability;  $A_{2avg}$  is the geometry average cross section area for section 2, which was also calculated with the bucket geometry as shown in formula A3.

$$A_{2avg} = \frac{\pi L}{3L_2(R_{out} - R_1)} \left\{ \left[ R_1 + \frac{L_2 + L_3}{L} (R_{out} - R_1) \right]^3 - \left[ R_1 + \frac{L_3}{L} (R_{out} - R_1) \right]^3 \right\} \quad (A3)$$